M. SAPIETA, A. SAPIETOVA, V. DEKYS

ISSN 0543-5846
METABK 56(1-2) 203-206 (2017)
UDC – UDK 669.15:539.43:536.51:620.16=111

COMPARISON OF THE THERMOELASTIC PHENOMENON EXPRESSIONS IN STAINLESS STEELS DURING CYCLIC LOADING

Received – Primljeno: 2016-08-10
Accepted – Prihvaćeno: 2016-11-25
Preliminary Note – Prethodno priopćenje

The main purpose of this paper is to compare the thermoelastic stress in specimens of stainless steel. As material specimens we chose stainless steel of AISI 304, AISI 316Ti and AISI 316L types. The specimens were cyclically loaded with three-point bending. The whole process was recorded using an infrared camera. The thermal differences that occurred during the test were evaluated based on the thermoelastic stress equations. Subsequently, stress distributions in the specimens were compared for different types of stainless steel.

Key words: stainless steel, cyclic loading, thermoelastic, stress distribution, infrared

INTRODUCTION

Nowadays, a combination of numerous infrared detectors or thermal sensors with advanced signal processing generates a practical tool for investigating thermal-stress characteristics of materials and structures from the respective surface or part of the space.

Thermoelastic stress analysis has been used by engineers and scientists for more than 50 years to address practical problems. It utilises the principle of sensing the energy released during loading in the elastic domain. Once loading is removed, the body returns to its original position (elasticity) and its original temperature (thermoelasticity) [1].

THERMOELASTICITY AND DISSIPATIVE TEMPERATURE VARIATION

Thermoelastic stress analysis (TSA) is an experimental contactless method based on measuring the infrared radiation emitted from the component surface exposed to dynamically linear elastic strain (deformation). Kelvin was the first scientist to study the thermoelastic effect, and the basic equations to describe the thermoelastic [2] effect were formulated by Darken and Curry.

The general form of the heat conduction equation for elastic body is derived from the energy conservation equation, and it can be written as follows:

$$\rho c_{\varepsilon}\frac{dT}{dt}-\frac{\partial}{\partial x_j}\left(k\frac{\partial T}{\partial x_j}\right)=\rho r+\sigma_{ij}\frac{\partial \varepsilon_{ij}}{\partial t}- \\ -\rho\frac{\partial \Psi}{\partial V_k}\frac{dV_k}{dt}+\rho T\frac{\partial^2\Psi}{\partial T\partial V_k}\frac{dV_k}{dt} \quad (1)$$

Equation (1) uses the Einstein summation convention, ρ is the density, c_ε is the specific heat capacity at constant deformation, T is the absolute temperature, k is the thermal conductivity tensor, σ_{ij} and ε_{ij} are the tensors of stress and strain, ε_{ij} is the inner heat source per unit of volume and ψ is Helmholtz free energy that is dependent on k and independent of the internal state variables V_k.

Provided that the material elastic properties and constant material coefficients are temperature independent, then it can be derived a 3-dimensional heat conduction equation written as follows:

$$\rho C_{\varepsilon}\dot{T}-k\Delta^2 T=T_0\left(-\frac{E\alpha}{1-2\upsilon}\right)\dot{\varepsilon}_1^e+\alpha_p\sigma_{ij}\dot{\varepsilon}_{ij}^p. \quad (2)$$

The equation for heat conduction will include the creation of the thermoelastic and the thermoplastic heat. Parameter $\dot{\varepsilon}_1^e$ denotes the first invariant of elastic deformation tensor $\dot{\varepsilon}_{ij}^p$ is the plastic part of the deformation tensor, α is the coefficient of thermal expansion, E Young's modulus, υ Poisson's ratio and T_0 is the initial temperature [3]. Non-dimensional coefficient α_p is the ratio of the total plastic work to plastic work, which is converted to heat. The value $\alpha_p \cong 1$ because of only a small part of the plastic work (obtained energy at cold forming) is used to change the inner properties of the material [4]. Therefor the thermoplastic area will be neglected and relationship will be formulated only for thermo-elastic area, which has the following form:

$$\Delta T=\frac{\alpha T_0}{\rho c_p}\Delta\sigma_{ii} \quad (3)$$

Where c_p is the specific heat capacity under constant pressure and its relationship with c_ε is as follows:

$$c_\varepsilon=c_p-\frac{2E\alpha^2 T}{\rho(1-\nu)} \quad (4)$$

M. Sapieta, A. Sapietova, V. Dekys, University of Žilina, Faculty of Mechanical Engineering, Department of Applied Mechanics, Žilina, Slovak Republic

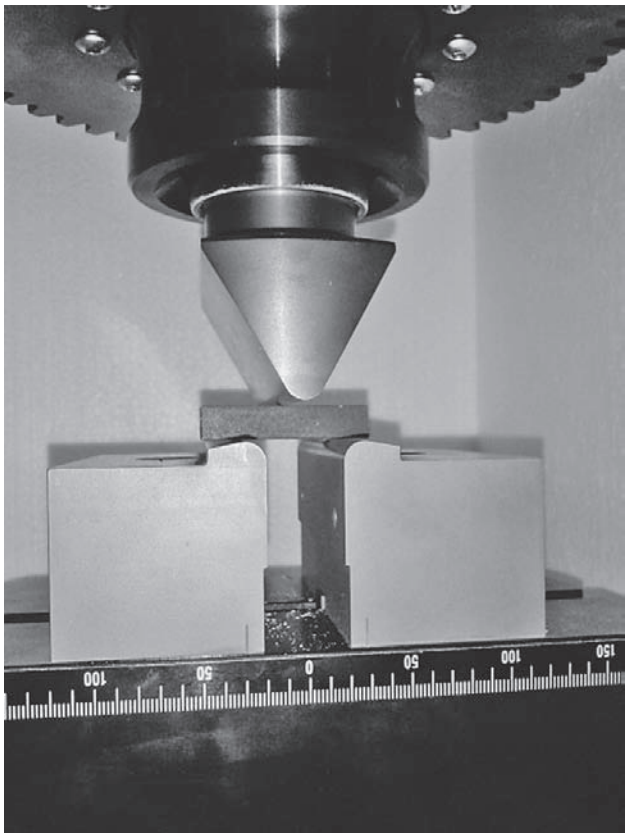

Figure 1 Specimen position during the three-point bending loading

STRESS ANALYSIS OF BEAMS MADE OF STAINLESS STEEL

Within this work it was carried out measurement of three-point bending of stainless steel beams. The specimen was 50 mm long and had a 10 x 10 mm square cross section. For this measurement it was chosen three types of material, namely: AISI 304, AISI 316L, and AISI 316TI.

The specimen was put on two supports and the loading forces acted from above onto the specimen centre between the supports (Figure 1). The supports were placed apart at a distance of 29 mm.

Again, it was chosen the infra-red camera maximum resolution 320 x 256 pixels, and corresponding frame rate 383 Hz. Loading frequencies differed for each material and each loading state – they fluctuated in the range of 100 - 105 Hz. Once again there was a slight subsampling. Since it was found from the previous measurements that this type of subsampling does not affect the quality of results, it chose that as the most suitable one in view of the resolution – sampling frequency ratio [5].

Material properties of individual specimens necessary for this type of analysis can be seen in Table 1.

In this case it was chosen 5 loading states for each specimen type. It chose more loading states because of better monitoring of the increase in stress with increasing loading force, and better comparison of individual material properties. Specimens were cyclically loaded

Table 1 **Input material properties required for the thermoelastic stress analysis of beams loaded with three-point bending**

Material	$\propto$ / K^{-1}	ρ / $K \cdot m^{-3}$	C_p / $J \cdot kg^{-1} K^{-1}$	K^{-1}/Mpa^{-1}
AISI 304	17,2 x 10^{-6}	7 900	502	4,34 x 10^{-6}
AISI 316L	16,5 x 10^{-6}	8 000	485	4,25 x 10^{-6}
AISI 316TI	16,6 x 10^{-6}	8 000	500,0	4,15 x 10^{-6}

Table 2 **Chosen loading states for three-point bending**

Loading state	1	2	3	4	5
Static component of force /kN	1	2	3	4	5
Dynamic component of force /kN	0,5	1	2	3	4

using a ZWICK testing machine. Loading took place gradually, from smallest to largest force. Table 2 shows the sizes of loading forces that was used.

It was always chosen a greater static component of the loading force Table 2 in order not to unburden the beam and to avoid displacement of the beam on the supports. In results it will be presented only first, third and fifth loading state.

THE RESULTS OF THERMOELASTIC ANALYSIS OF THE AISI 304 MATERIAL SPECIMENS

Substituting the material properties of this type of material it was achieved the following distributions of stress fields (Figures 2–4). In this type of loading, considerably noised areas are no longer distinct even at lower loads, which was the case in tensile loading. It could however be said that at the maximum load the image is sharper, unlike the image at the minimum load.

Also the sum of principal stresses grows with increasing loading. The loading finger is located above

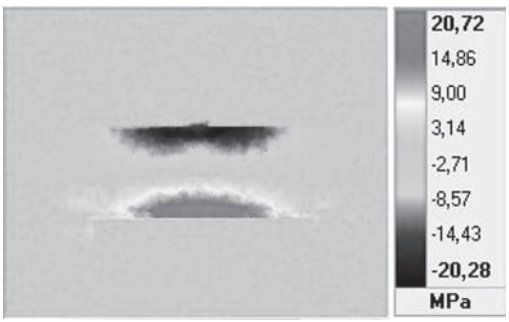

Figure 2 Distribution of principal stresses in the beam AISI 304 specimen at 0,5 kN loading

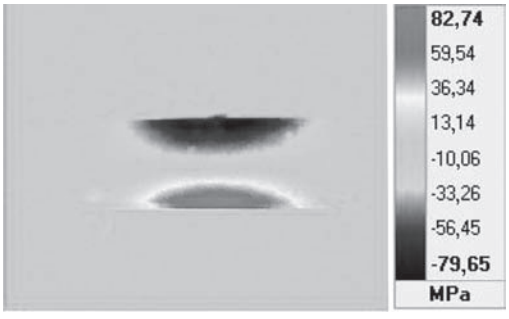

Figure 3 Distribution of principal stresses in the beam AISI 304 specimen at 2 kN loading

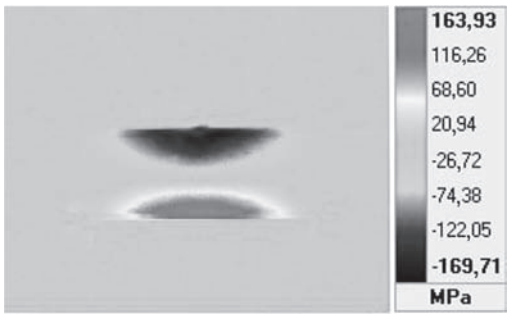

Figure 4 Distribution of principal stresses in the beam AISI 304 specimen at 4 kN loading

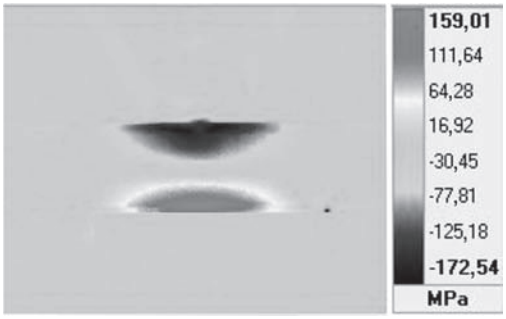

Figure 7 Distribution of principal stresses in the beam AISI 316L specimen at 4 kN loading

the upper part of the specimen, and the minimum stress value (negative) there is shown in blue, which represents compressive stressing of the longitudinal fibres. The lower part of the specimen – the area between the supports – is shown in red, which represents tensile stressing of the longitudinal fibres.

The maximum stress value is situated in the lower part and shown in purple, and the minimum stress value is situated in the upper part and shown in dark blue.

THE RESULTS OF THERMOELASTIC ANALYSIS OF THE AISI 316L MATERIAL SPECIMENS

The second material to be loaded was the AISI 316L specimen. In this type of material, it can be observed slightly noised areas (yellow area above the left-hand side support) even at lower loading (Figure 5). Nevertheless, these noised areas do not reach the level that was the case of tensile loading. Another anomaly, unlike in measurements of other specimen types, is the spot-sized dark blue area on the right side above the right-hand side support. This dark blue spot occurs in all loading states only in this material type. It could be explained by incorrect positioning.

All in all, the stress and image sharpness increase with increasing load, which can be evaluated as a positive property. The upper part under the loading finger features the minimum stress shown in dark blue, and in the lower part between the supports it can be seen the maximum stress shown in purple.

THE RESULTS OF THERMOELASTIC ANALYSIS OF THE AISI 316TI MATERIAL SPECIMENS

The last material to be loaded with three-point bending was the AISI 316TI specimen. The measurement and evaluation were carried out in the same manner as in the previous two cases. Slightly noised areas can be seen in the first image (Figure 8).

The stress value increases with increasing load. Identically to the previous measurements, the maximums and minimums are situated in the same areas.

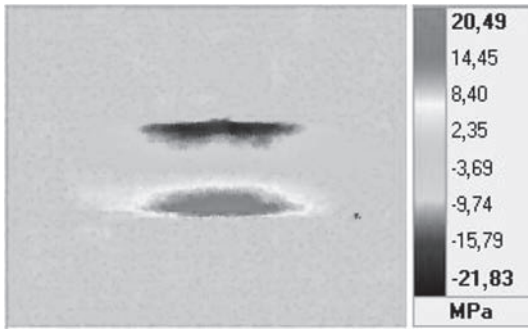

Figure 5 Distribution of principal stresses in the beam AISI 316L specimen at 0,5 kN loading

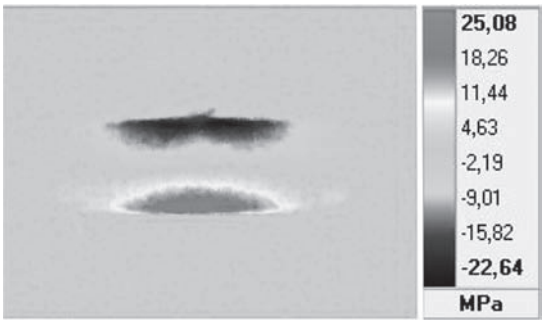

Figure 8 Distribution of principal stresses in the beam AISI 316TI specimen at 0,5 kN loading

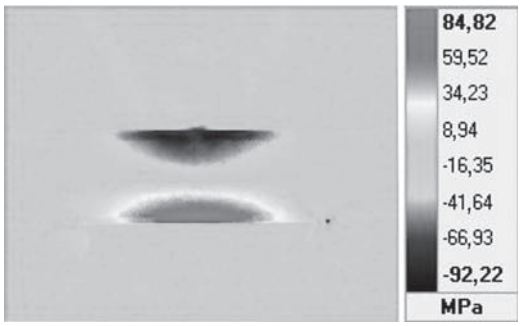

Figure 6 Distribution of principal stresses in the beam AISI 316L specimen at 2 kN loading

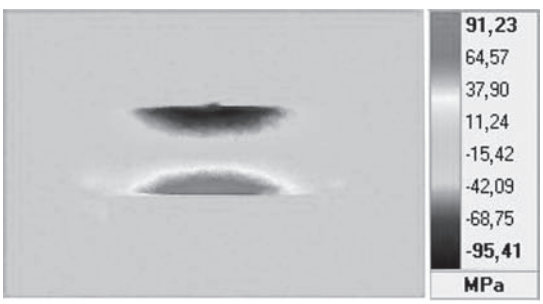

Figure 9 Distribution of principal stresses in the beam AISI 316TI specimen at 2 kN loading

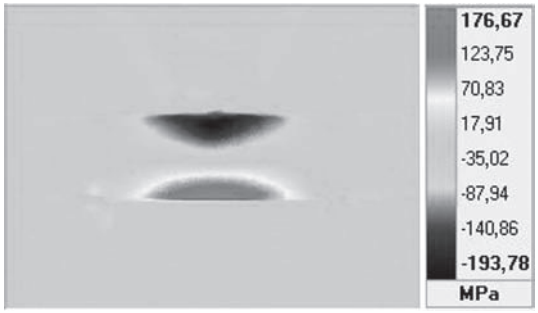

Figure 10 Distribution of principal stresses in the beam AISI 316TI specimen at 4 kN loading

Aside from this minor shortcoming, all the three types of images with those materials can be considered symmetrical in the vertical plane, which is perpendicular to the specimen cross-section.

CONCLUSIONS

For this measurement it was chosen 3 types of specimens with identical geometry and different material properties, making it possible to compare the impact of individual material properties on the stress field distribution. It could be observed changes in the stress field distribution and max – min value of stress depending on changed specimen material at constant loading levels. Differences between values of stress levels are minimal. The biggest difference between materials consists in the minimum of stress which is displayed by blue colour on the top of the specimens. On the basis of this measurement it can be concluded that this method is suitable for further use in the elastic domain.

Acknowledgements

This work has been supported by the grant projects VEGA No. 13/010/00.

REFERENCES

[1] V. Vavilov, Thermal / Infrared testing. In: Nondestructive testing, Publishing house Spektr, (2009). – 732p.

[2] V. Dekys, P. Kopas, M. Sapieta, A detection of deformation mechanisms using infrared thermography and acoustic emission. Novel trends in production device and systems. Book series: Applied Mechanics and Materials. 474 (2016), 315-320.

[3] P. Pecháč, M. Sága, Controlling of Local search Methods' Parameters in Memetic Algorithms Using the Principles of Simulated Annealing, Procedia Engineering, 136 (2016), 70-76.

[4] X.P.V. Maldague, Theory and Practice of Infrared Technology for Nondestructive Testing.Wiley, New York 2001

[5] J. Awrejcewicz, Y. Pyryev, Thermoelastic contact of a rotating shaft with a rigid bush in conditions of bush wear and stick-slip movements, International Journal of Engineering Science, (2002), 59-64.

Note: The responsible translator for the English language is Súkeníková, Sarja, Žilina, Slovakia